JOURNAL OF MATERIALS SCIENCE 25 (1990) 1603–1609

The mechanical properties of laminated microscale composites of Al/Al_2O_3

A. T. ALPAS, J. D. EMBURY
Department of Materials Science and Engineering, McMaster University, Hamilton, Ontario, Canada, L8S 4L7

D. A. HARDWICK, R. W. SPRINGER,
Materials Science and Technology Division, Los Alamos National Laboratory, Los Alamos, New Mexico, USA 87545

The tensile properties, at both room and elevated temperatures, of laminated thin films containing alternate layers of aluminium and aluminium oxide were investigated. At room temperature the strength of the films followed a Hall–Petch type relationship dependent on the interlamellar spacing, and the strength could be extrapolated from data for conventional grain size aluminium. At the finest interlayer spacing of 50 nm, the strength was equivalent to $\mu/70$, where μ is the shear strength of aluminium and the samples exhibited very extensive ductility. At elevated temperatures, cavitation became an important deformation mechanism but it occurred preferentially at Al/Al rather than Al/Al_2O_3 boundaries. The microstructure of the films was probed using transmission electron microscopy and fractography was used to investigate deformation and fracture mechanisms.

1. Introduction

New processing routes such as vapour deposition and sputtering enable composites to be fabricated in which the intrinsic scale of the microstructure is extremely fine (of the order of 5–500 nm). The study of the mechanical response of such laminates is of considerable interest from both a basic and an applied viewpoint. Such structures are of value in helping to delineate the range of applicability of known strengthening mechanisms and the morphological stability of fine scale structures.

In the present study laminated composites of Al/Al_2O_3 were prepared in an electron beam deposition system using a pulsed gas process [1]. As 99.999% pure aluminium was evaporated, at a rate of approximately 3.5 nm sec^{-1}, onto a Csl-coated glass slide, oxygen was pulsed into the vacuum system producing an oxygen-containing layer at predetermined intervals. These alternating layers of aluminium and aluminium oxide were deposited until the specimens reached an overall thickness of $25 \pm 3\,\mu m$. The resulting laminates had interlayer spacings ranging between 50 and 500 nm. The aluminium oxide was approximately 5 nm thick and had a composition close ot Al_2O_3 but substoichiometric with respect to oxygen [2].

2. Experimental details

2.1. Microstructural characterization

Cross sections of the laminates were prepared for TEM examination by both microtoming and ion milling methods while samples within the plane of the foil were produced electrochemically. TEM observations were made using either a Phillips CM 12 or a Phillips 400T. The texture of the composites was determined by X-ray diffraction for both the as-fabricated condition and after annealing at 723 K for 1 h.

2.2. Tensile tests

Tensile tests on very thin samples often exhibit premature failure due to tearing from the edges and alignment problems. In order to minimize the problem, 20 mm × 10 mm pieces of the material were clamped between aluminium plates and a reduced gauge section, 6 mm long and 3.5 mm wide, was machined. Prior to testing, all samples were examined with an optical microscope to determine that the sample edges were smooth. In addition, a clamping arrangement was devised to ensure the self-alignment of specimens during tensile testing.

Tensile tests were performed at 297, 577 and 683 K at strain rates varying between 10^{-2} and 10^{-4} sec^{-1}. A screw-driven Instron machine was used for the tests at 297 and 577 K while tests at 687 K were performed using a servohydraulic MTS machine. Both machines were fitted with a load cell of maximum capacity 500 N. The furnace temperature in the elevated temperature tests was controlled to within ± 5 K of the desired value. The data points reported here represent the average of three tests at each temperature and strain rate. Fractography was performed using a Phillips 501 scanning electron microscope.

Attempts were made to obtain strain rate sensitivity data by making stepwise changes in cross-head velocity and noting the change in stress level. However, at higher temperatures, the reproducibility

0022–2461/90 $03.00 + .12

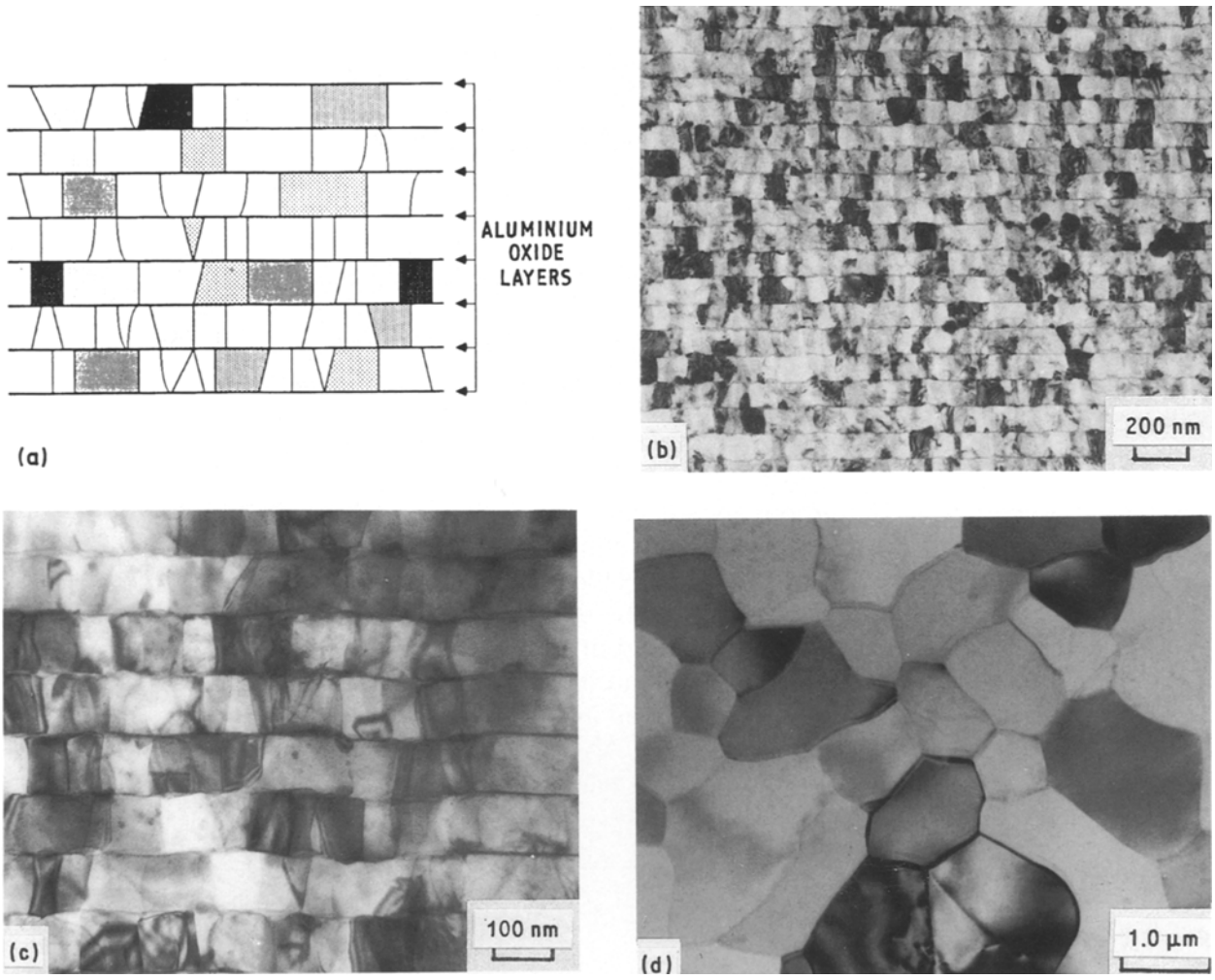

Figure 1 Microstructure of the laminates: (a) schematic representation of laminate cross-section, (b) microtomed cross-section, (c) ion-milled cross-section, and (d) parallel to plane of laminate.

of the data was such that definite values of the rate sensitivity could not be obtained. Thus, strain rate sensitivity could not be used to delineate changes in deformation mode with temperature or interlamellar spacing.

2.3. Tear tests

In order to obtain a comparative measure of the fracture resistance of these microscale composites, tear tests of the type devised for polymers by Rivlin and Thomas [3] were used. Rectangular samples, 20 mm × 8 mm × 25 μm, with a 6 mm long initial slit were used. The tear energy per unit area, Γ, was calculated from the relationship:

$$\Gamma = 2F/t$$

where F is obtained from the tear force/crack extension curve for a 10 mm extension and t is the sample thickness. Tests were performed at 298 K at a tear rate of 4×10^{-3} mm sec^{-1}.

3. Results

3.1. Microstructure

The form of the laminates after fabrication is shown schematically in Fig. 1a. The periodicity of the structure is illustrated by Fig. 1b which was obtained from a microtomed cross-section, while Fig. 1c taken on an ion-milled cross-section, clearly shows the oxide between the aluminium layers. Sections prepared parallel to the layers, Fig. 1d, show that the grains are essentially flat discs that are equiaxed in the plane of the laminate with diameters of the order 0.5–2.0 μ.

The as-fabricated composite exhibited a weak (1 1 1) texture. After annealing, a sharpening of this (1 1 1) texture was observed; this may result from the elimination of smaller grains.

3.2. Mechanical response at ambient temperature

Tensile tests at room temperature showed that the flow stress, σ_f, of the composites increased with decreasing interlameller spacing, as shown in Fig. 2. This plot includes results from both the as-fabricated material and material which was subjected to an anneal at 738 K for 24 h prior to testing. The elastic–plastic transition in these materials was not sharp and the flow stress values were obtained after 2% elongation. The data can be replotted in the formalism of the Hall–Petch equation [4, 5]:

$$\sigma_f = \sigma_0 + k\lambda^{-1/2}$$

where σ_0 is a friction stress, λ is the interlamellar spacing between Al_2O_3 layers, and k is a constant indicative of the barrier strength. Such a plot is shown

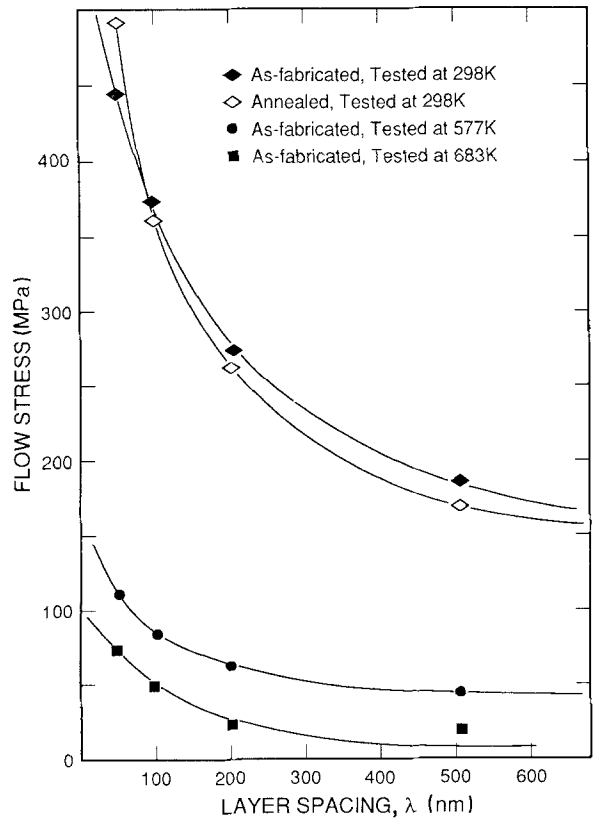

Figure 2 Flow stress, as a function of interlamellar spacing, of as-fabricated and annealed laminates tested at 297 K and of as-fabricated laminates tested at 577 K and 683 K.

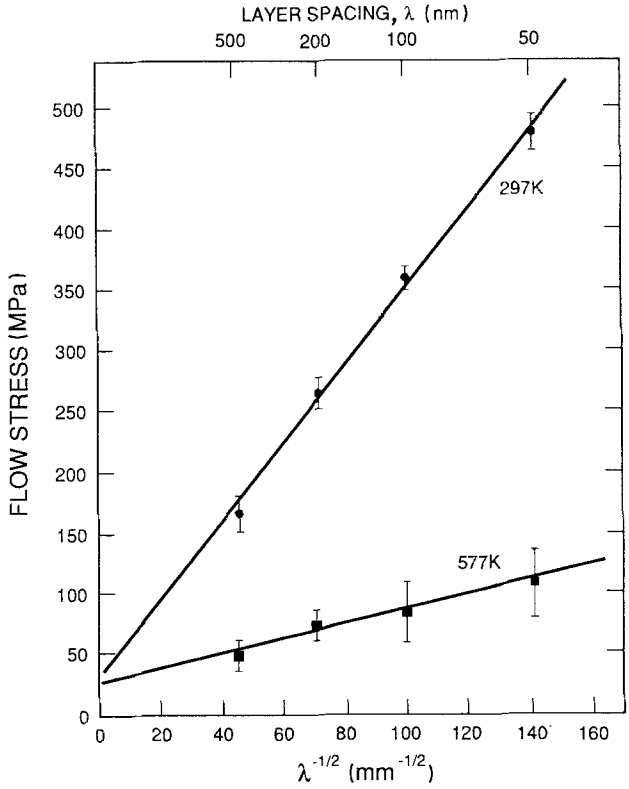

Figure 3 Hall-Petch plot of the results from samples tensile tested at 297 K and 577 K.

in Fig. 3. The results indicate three salient features of the mechanical response of the composites:

(i) the dominant factor governing the strength appeared to be the interlamellar spacing;

(ii) the strength level was unchanged by annealing at 738 K for 24 h indicating that the fine scale lamellar structure was thermally stable;

(iii) the highest strength level obtained (for $\lambda = 50$ nm) was ≈ 450 MPa which is approximately $\mu/70$, where μ is the shear modulus of aluminium.

At room temperature the samples necked and exhibited two forms of final failure – fracture via dimple formation and necking to a line, as shown in Figs 4a and 4b. The tendency to neck to a line with no dimple production was greatest in samples of largest interlamellar spacing, i.e. lowest stress level.

3.2. Mechanical response at elevated temperatures

The flow stress of the material at elevated temperatures was much lower and showed less dependence on the interlamellar spacing than at room temperature. This is illustrated in Figs 2 and 3.

The fracture behaviour and fracture morphologies were related to the interlamellar spacing as shown in Figs 5a and 5b. Fracture in samples with an interlamellar spacing of 50 nm appeared to involve ductile fracture with dimples of the order of 0.2–1.0 μm (Fig. 5a). For samples with interlamellar spacings of 100–500 nm, the fracture surfaces showed features which suggested that some structural features developed during high temperature flow which penetrated through the thickness of the composite or some large fraction of it.

The specimen surface, when examined in the plane of the laminate, showed evidence of cavitation which appears to occur co-operatively with the deformation process, as shown in Fig. 6a. The cavitation events are localized but can penetrate through the thickness of the laminate and lead to fracture as shown in Fig. 6b. This result indicates that high temperature flow involves damage by cavitation and that it is the spatial co-ordination of damage events which leads to failure.

3.3. Evaluation of fracture resistance

The values of Γ, the tear energy per unit area, reported in Table I represent the average of four tests for each lamellar spacing. It should be noted that the values of the tear energy per unit area increase with increasing flow stress. The work done by the applied stress in a tear test is consumed in a complex way both by ligament bending and by the plastic work of the fracture process, so that in ductile metals, Γ, is a function

TABLE I Tear energies (Γ) of Al/Al_2O_3 composites

λ (nm)	Tear energy per unit area Γ (kJ m^{-2})	Flow stress σ (MPa)	Fracture mode
50	12.0	450	Necking to a line and ductile fracture
100	10.4	380	Necking to a line
500	5.8	180	Necking to a line

TABLE II Comparison of Hall–Petch parameters

Material	σ_0 (MPa)	k (MPa m$^{1/2}$)	Grain size range (μm)	Reference
Al/Al_2O_3 laminate	80.7	0.10	0.005–0.5	–
99.97% Al	11.0	0.07	30–100	7
99.99% Al	5.5	0.04	80–100	8
99.99% Al	22.4	0.07	30–100	9
1100 Al	14.3	0.07	20–200	10

of sample thickness [6]. The values of Γ reported in Table I are for samples of constant thickness and therefore are only comparative, not absolute values of fracture resistance. However, the observation that the failure occurs predominantly by necking to a line suggests that both the strain levels and the volume involved in fracture are essentially independent of lamellar spacing and hence the tear energies should increase with flow stress as observed.

4. Discussion

Consider first the behaviour of the microscale composites at room temperature. As the volume fraction of the aluminium oxide is only of the order of 8% and the material is polycrystalline in the plane of the laminate, it is appropriate to consider the strengthening as being due to grain refinement rather than dispersion or fibre strengthening. The data can be plotted in the form of a Hall–Petch plot as shown in Fig. 3. It is appropriate to comment on the selection of the Hall–Petch formalism to represent the data. The observation in several samples of necking to a line which was parallel to the deposited layers indicates that deformation is transferred across the layers rather than by the co-operative shuttling of dislocations constrained within the Al by the Al_2O_3 layers for which the λ^{-1} dependence of the Orowan strengthening mechanism would be appropriate. The data is compared with existing data for polycrystalline aluminium [7–10] in Table II which indicates that the strength of the laminates can be related to the data for conventional grain sizes. As the range of interlamellar spacing in the current tests is limited, it is difficult to compare quantitatively the values of the Hall–Petch slopes and relate them to the detailed mode of slip transfer. However, as the Al_2O_3 is of the order of 5 nm in thickness and may be amorphous, it is probable that the local stresses needed to penetrate these layers are of the same order as those necessary for slip transfer at conventional grain boundaries. It appears that the interlamellar spacing controls the strength even though the dimensions of the grains in the plane of the laminate are an order of magnitude greater in size.

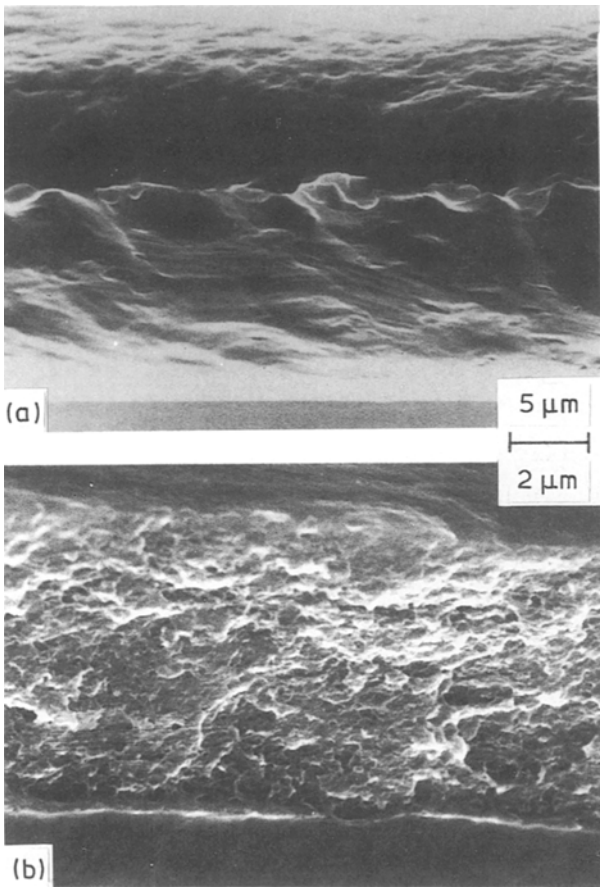

Figure 4 Fractographs of samples tested to failure at ambient temperature illustrating: (a) laminate failure by necking to a line, and (b) laminate failure by ductile rupture.

The detailed mechanism of slip transfer across the oxide layers cannot be elucidated from the current study. It may be aided by the diffuse nature of the Al/Al_2O_3 interface but it must take place without the production of significant delamination or dilatational damage in order for the samples to neck to a line as shown in Fig. 4a. The use of deposited microscale laminates may provide a unique method of studying the detailed slip transfer process at boundaries. In future studies, through variation of the thickness of the Al_2O_3 layers and control of the diffuse nature of the interface, it should be possible to define the conditions for slip transfer and decohesion at Al/Al_2O_3 interfaces.

The level of strength attained by these fine scale laminates (up to 450 MPa) is higher than for most aluminium alloys strengthened by precipitation of second phase particles. The combination of strength, ductility and tear resistance exhibited by these microscale composites at ambient temperatures and their thermal stability suggests that vapour deposition may be a valuable method for the production of ultra-high strength materials for specific applications.

With respect to the material behaviour at elevated temperatures, the observations indicate that cavitation within the Al layers is an important process. In samples with interlamellar spacings of 500 nm, the cavitation becomes spatially organized in the form of bands, in a manner analogous to shear bands as shown in Fig. 6a. Organization of the cavitation can also occur in the through thickness direction. This

result suggests that cavitation on the Al/Al_2O_3 boundaries is significantly more difficult than at the Al/Al boundaries within a layer. This may be a reflection of the fact that the fabrication method does not produce a sharp delineation between the Al and the Al oxide layers; Auger spectroscopy has established that oxygen gradients exist at this interface [1]. Also, the spread of cavitation is retarded by the Al/Al_2O_3 boundaries, as shown in Fig. 7, so that the cavitation can spread through an appreciable fraction of the total thickness of the laminate only at the higher interlamellar spacings.

In the samples with the finest interlamellar spacing there was no evidence of bands of cavitation or extensive through thickness organization. Thus, the fracture surface shown in Fig. 5a consists of 0.2–1.0 μm dimples.

The results indicate that during flow at elevated temperatures, cavitation occurs in a co-operative manner producing strain localization and damage which leads to failure. However, the extent of this spatial organization is dependent on the interlamellar spacing. The Al/Al oxide boundaries are resistant to damage which suggests that extended interfaces of this type may be of value for controlling the spread of damage in high temperature materials.

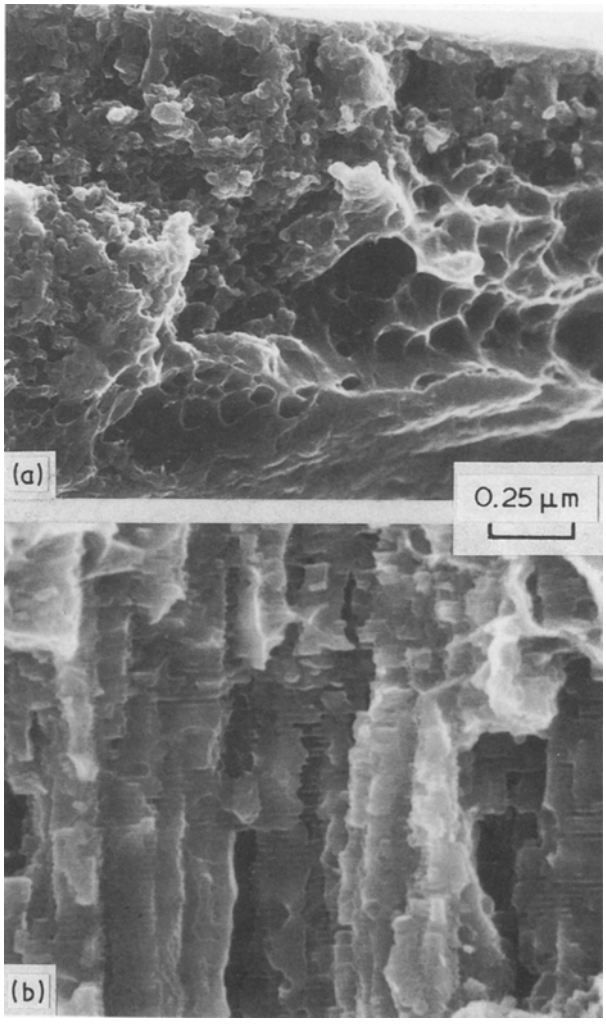

Figure 5 Fractographs of samples tested to failure at elevated temperature: (a) laminate spacing, $\lambda = 50$ nm and (b) laminate spacing, $\lambda = 200$ nm.

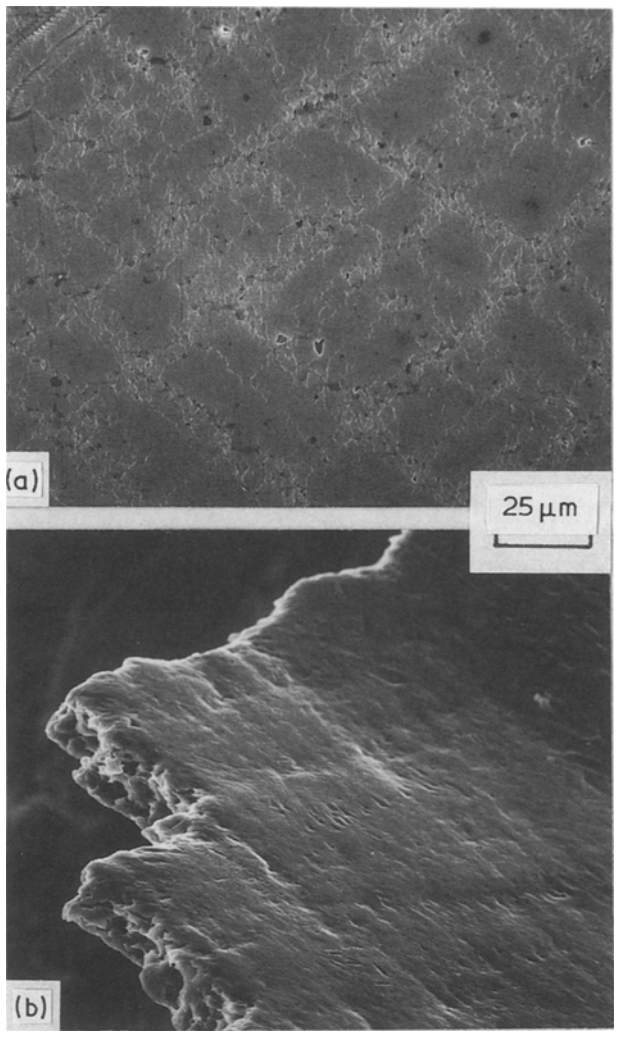

Figure 6 (a) Specimen surface after elevated temperature deformation, and (b) interaction of specimen surface features and fracture surface.

It would be advantageous to be able to construct a deformation mechanism map [11] for these laminated films, analogous to that constructed by Murakami for lead films [12]. Such a map would allow the prediction of the dominant mechanism of plastic flow at a given stress and temperature. However, the deformation of these laminated films is complicated by the fact that

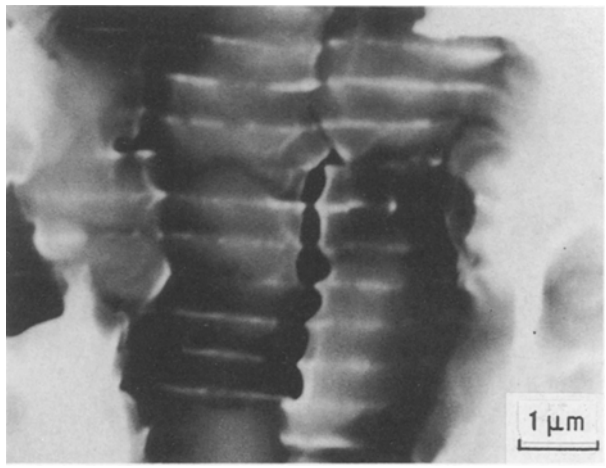

Figure 7 High magnification fractograph showing retardation of cavitation at the Al/Al_2O_3 boundaries.

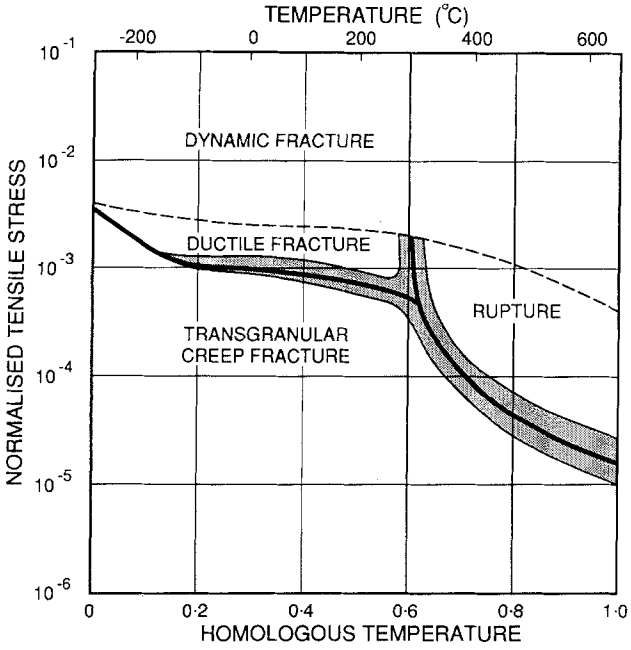

Figure 8 Fracture map for high purity aluminium of conventional grain size, after [13].

the Al/Al_2O_3 and the Al/Al boundaries do not behave in the same manner. Thus the deformation behaviour is dependent on lamellar spacing and difficult to represent in the form of a map.

The fracture modes of these microscale laminates are complex because the Al/Al and Al/Al_2O_3 interfaces exhibit different propensities for cavitation. Further, the spatial organization of cavitational damage is dependent on the lamellar spacing of the composites. Thus if the classification of failure modes is considered in the form of a fracture mechanism map (Fig. 8) of the type proposed by Ashby *et al.* [13], no quantitative comparison can be made with pure Al of conventional grain size. However, it is of value to outline the observed modes of failure despite the limited amount of data available from the current study. This has been done in Fig. 9. It can be seen that the presence of two types of interface introduces new fields into the fracture mechanism map. Clearly, the current data does not provide a definitive evaluation of the fracture mechanisms map for microscale composites, but it does indicate that further work in the

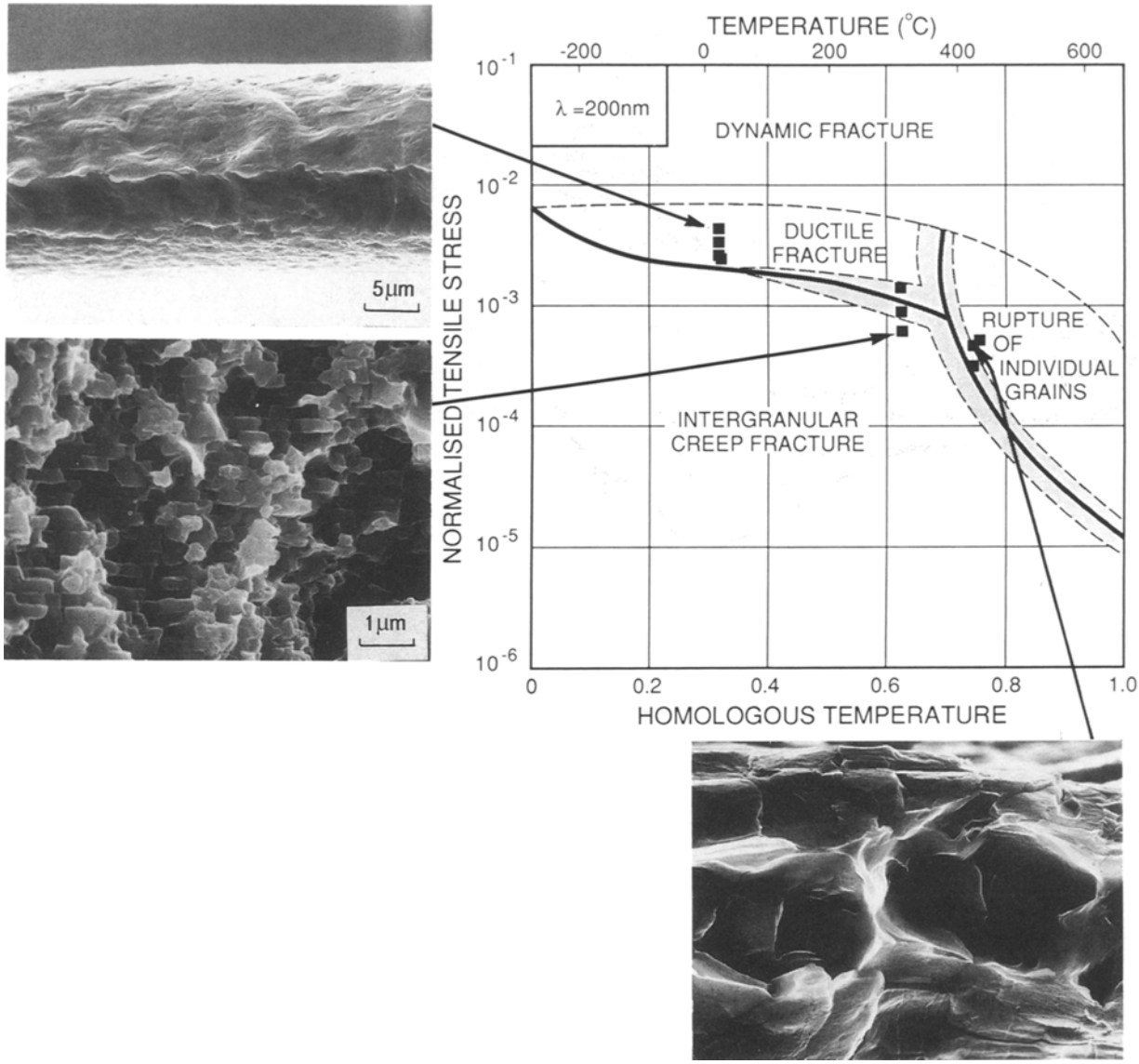

Figure 9 Fracture map for the Al/Al_2O_3 laminate films with an interlamellar spacing of 200 nm.

area may prove valuable in elucidating the useful range of applications for microscale laminates.

5. Conclusions

The current work indicates that microscale composites of Al/Al_2O_3 can develop strength levels of the order of $\mu/70$ together with useful ductility and tear resistance. The results show that the Al/Al_2O_3 boundaries are extremely resistant to decohesion and cavitation over a range of temperatures and that the damage processes at Al/Al and Al/Al_2O_3 boundaries are markedly different. The composites described in this study retain their strength levels despite exposure at high temperatures, and thus represent a useful approach to the development of high strength materials for some structural applications.

Acknowledgements

The authors would like to thank Dr A. D. Rollett of Los Alamos National Laboratory for the texture determinations and Mrs T. Castillo of McMaster University for preparation of microtomed electron microscopy samples. The authors wish to acknowledge NSERC, Canada (A.T.A. and J.D.E.), Los Alamos National Laboratory (D.A.H. and R.W.S.) for support during the period of this work. They would also like to thank J. P. Hirth and F. Spaepen for critical reading of the manuscript. This paper constitutes work performed under the auspices of the US Department of Energy.

References

1. R. W. SPRINGER and D. S. CATLETT, *Thin Solid Films* **54** (1978) 197.
2. D. A. HARDWICK, C. J. MAGGIORE and R. W. SPRINGER, *Nucl. Instrum. Meth.* **B15** (1986) 260.
3. R. S. RIVLIN and A. G. THOMAS, *J. Polym. Sci.* **10** (1953) 291.
4. E. O. HALL, *Proc. Phys. Soc., Lond.* **B64** (1951) 747.
5. N. J. PETCH, *J. Iron and Steel Inst.* **174** (1953) 25.
6. A. T. ALPAS, L. EDWARDS and C. N. REID, *Acta Metall.* **35** (1987) 787.
7. R. P. CARREKER and W. H. HIBBARD, *Trans. AIME* **209** (1957) 1157.
8. N. HANSEN, *Acta Metall.* **25** (1977) 863.
9. H. FUJITA and T. TABATA, *Acta Metall.* **21** (1973) 355.
10. A. W. THOMPSON and M. I. BASKES, *Phil. Mag.* **28** (1973) 301.
11. M. F. ASHBY, *Acta Metall.* **20** (1972) 887.
12. M. MURAKAMI, *Thin Solid Films* **55** (1978) 101.
13. M. F. ASHBY, C. GANDHI and D. M. R. TAPLIN, *Acta Metall.* **27** (1979) 699.

Received 18 January
and accepted 7 June 1989